U. S. DEPARTMENT OF COMMERCE
Luther H. Hodges, Secretary
WEATHER BUREAU
F. W. Reichelderfer, Chief

NATIONAL SEVERE STORMS PROJECT

REPORT No. 11

A Report of the Kinematic Properties of Certain Small-Scale Systems

by
Dansy T. Williams
National Severe Storms Project, Kansas City, Mo.

Washington, D. C.
October 1962

CONTENTS

		Page
	ABSTRACT	1
1.	INTRODUCTION	1
2.	THE KINEMATIC PROPERTIES	2
3.	MEASUREMENTS AND ANALYSES	3
4.	THE CASE OF MARCH 19, 1948	3
5.	THE CASE OF AUGUST 29, 1948	10
6.	THE CASE OF APRIL 7, 1948	15
7.	SUMMARY	19
	A. General Features	19
	B. Specific Features of the Squall Line	20
	C. Specific Features of the Isolated Thunderstorm	20
	D. Specific Features of the Depression Wave Line	21
8.	ACKNOWLEDGMENTS	21
	REFERENCES	22

A STUDY OF THE KINEMATIC PROPERTIES OF CERTAIN SMALL-SCALE SYSTEMS*

Dansy T. Williams
National Severe Storms Project
U. S. Weather Bureau
Kansas City, Missouri

ABSTRACT

Small-scale computations of surface divergence, vorticity, deformation, and Petterssen's frontogenetical function were made with respect to a squall line, an isolated thunderstorm, and a depression wave line. The leading edge of the squall line was found to lie along an axis of maximum convergence, deformation, and frontogenesis. Centers of maximum convergence, deformation, and frontogenesis, were found in the vicinity of a micro-low along the leading edge of the squall line. Kinematic properties with respect to the depression wave were comparatively weak and poorly defined. They were strong and well defined with respect to the center of the isolated thunderstorm and the pseudo-cold fronts enclosing it. The kinematic properties of the systems give some indication as to the immediate short-period mechanisms responsible for the growth and decay of the systems.

I. INTRODUCTION

The horizontal wind field of a weather system provides a basis for deriving the kinematic properties of the system. Kinematic properties of large-scale systems are rather well known, and such properties as divergence and vorticity are routinely used in forecasting. The kinematic properties of smaller-scale systems are less well known. It is the purpose of this paper to describe the kinematic properties of three such systems: (1) a squall line, (2) an isolated thunderstorm, and (3) a depression wave line. The studies are individual cases.

The wind, pressure, and temperature discontinuities of small-scale systems can be likened to those of large-scale frontal systems; and their associated small-scale Lows, Highs, troughs, and ridges can be likened to their large-scale counterparts. When this is done, it is found that the kinematic properties of one resemble those of the other, except that the intensity and rate of change for the small-scale systems is 2 to 3 orders of magnitude greater than for the large-scale systems.

* Presented at the Conference on Severe Storms, Norman, Oklahoma, February 13-15, 1962.

The cases have been selected from the 1948 surface network data of the U. S. Weather Bureau's Cloud Physics Project, Wilmington, Ohio. The stations in this network were spaced in checkerboard fashion at approximately 2-mile intervals. This compact spacing has permitted analysis on a scale that approaches that of the systems studied. These rather old data have been used, since the cases were considered worthy, and since there are very few recent data of comparable quality on so small a scale.

2. THE KINEMATIC PROPERTIES

The horizontal space derivatives of the horizontal wind are: $\partial u/\partial x$, $\partial v/\partial y$, $\partial v/\partial x$, and $\partial u/\partial y$. By combining these as various sums the following kinematic properties of the horizontal flow are expressed:

$$\partial u/\partial x + \partial v/\partial y = Div_2\ \mathbf{V}, \text{ horizontal velocity divergence} \quad (1)$$

$$\partial v/\partial x - \partial u/\partial y = Rot_2\ \mathbf{V}, \text{ vertical component of relative vorticity} \quad (2)$$

$$\partial u/\partial x - \partial v/\partial y = Def_2\ \mathbf{V}, \text{ horizontal stretching deformation} \quad (3)$$

$$\partial v/\partial x + \partial u/\partial y = Def'_2\ \mathbf{V}, \text{ vertical component of horizontal shearing deformation} \quad (4)$$

The absolute magnitude of the resultant deformation, $Def_R\ \mathbf{V}$, and the axes along which dilatation and contraction occur are generally more meaningful than the stretching and shearing deformations given in equations (3) and (4). These equations can be transformed to yield $Def_R\ \mathbf{V}$, as:

$$Def_R\ \mathbf{V} = Def_2\ \mathbf{V} \sec 2\phi \quad (5)$$

where:

$$2\phi = \tan^{-1}(Def'_2\ \mathbf{V} / Def_2\ \mathbf{V}) \quad (6)$$

Algebraic signs of $Def_2\ \mathbf{V}$ and $Def'_2\ \mathbf{V}$ can then be used with values of ϕ to yield the dilatation and contraction axes. A procedure for doing this has been outlined by Saucier [1].

Frontogenesis is favored along axes of maximum horizontal convergence and along axes of greatest deformation dilatation. It is also required that a density gradient be present. Petterssen [2] has defined a frontogenetical function

$$F = \tfrac{1}{2} |\nabla\theta| (Def_2\ \mathbf{V} \cos 2\beta - Div_2\ \mathbf{V}), \quad (7)$$

where:

$\nabla\theta$ = absolute magnitude of potential temperature gradient

$Def_2\ \mathbf{V}$ = horizontal stretching deformation

Div_2 **V** = horizontal velocity divergence

β = the angle between the axis of dilatation and the potential temperature isotherms

Positive values of F indicate frontogenesis, negative values indicate frontolysis.

3. MEASUREMENTS AND ANALYSES

Surface wind analyses were made for appropriate stations in the network, using the continuously recorded wind directions and wind speeds. In the analyses the winds were decomposed into their u- and v- components, and from isotach analyses of these components the horizontal space derivatives were measured. These were approximated by the finite differences, $\delta u/\delta x$, $\delta v/\delta y$, $\delta v/\delta x$, and $\delta u/\delta y$, with the measuring intervals, δx and δy taken as 2 statute miles. Measurements were made at the interior stations of the network and at the centroids of the quadrangles formed by all stations of the network. The various kinematic properties were obtained by substituting measured values of the space derivatives in equations (1) through (6). Values of the properties were obtained in units of $hr.^{-1}$ For a conversion to units of $sec.^{-1}$, one may note that 3.6 $hr.^{-1}$ is equal to 10^{-3} $sec.^{-1}$.

Isotherm analyses were made from plotted values of temperature, with isotherms drawn for every whole degree Fahrenheit. These were used to determine ∇T, the gradient of temperature. ∇T was used in place of $\nabla\theta$ in equation (7), it being assumed that the two were approximately proportional. The approximation neglects the differences in station elevations, and the gradients of pressure. The maximum possible error of the approximation was 1°F/2 mi. Since temperatures were read only to the nearest 1°F., and since actual gradients as great as 13°F./2 mi. were measured, the approximation is considered to be sufficiently good for the cases studied. ∇T and β were measured from the isotherm analyses and plots of the dilatation axes of deformation. These values were substituted with values of Div_2 **V** and Def_2 **V** in equation (7) to yield values of F.

4. THE CASE OF MARCH 19, 1948

This was a pre-cold-frontal squall line which produced damaging winds over the northern portion of the network. Various features of this case have been reported previously [3, 4, 5]. Surface synoptic charts with plotted winds and sea-level isobars at 1400 and 1405 EST are shown in figures 1 and 2. Wind speeds are in m.p.h. with a whole barb equal to 10 m.p.h. and a pennant equal to 50 m.p.h. Isobars are drawn at intervals of 1 mb. The features of interest are the leading edge of the squall line (indicated by cold front symbols), the micro-low along the leading edge, the micro-high to the rear of the leading edge, and a corridor 1 to 2 miles wide (not indicated in the figure) about 2 miles in advance of the leading edge.

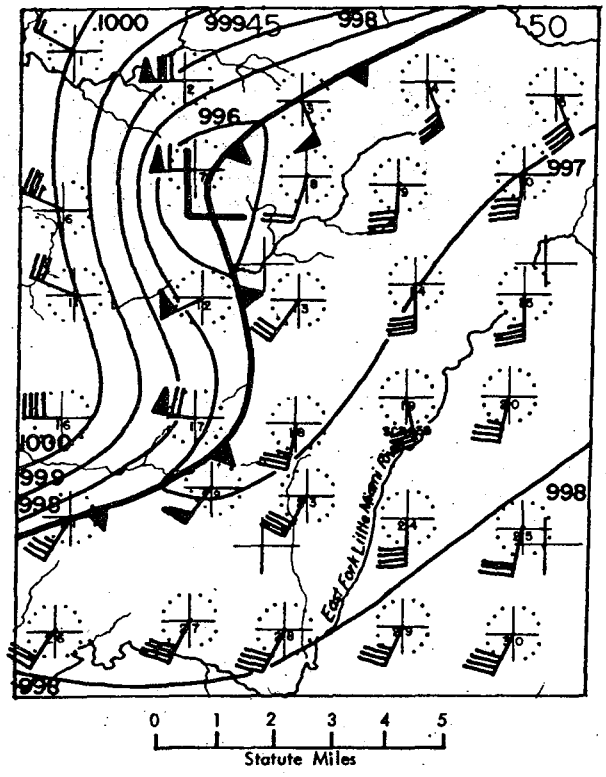

Figure 1 - Surface wind and pressure, 1400 EST, March 19, 1948.

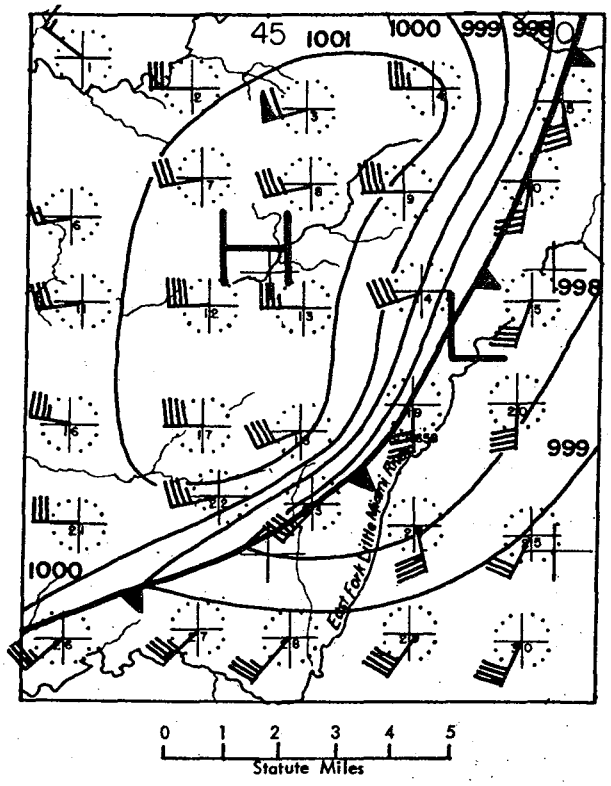

Figure 2 - Surface wind and pressure, 1405 EST, March 19, 1948.

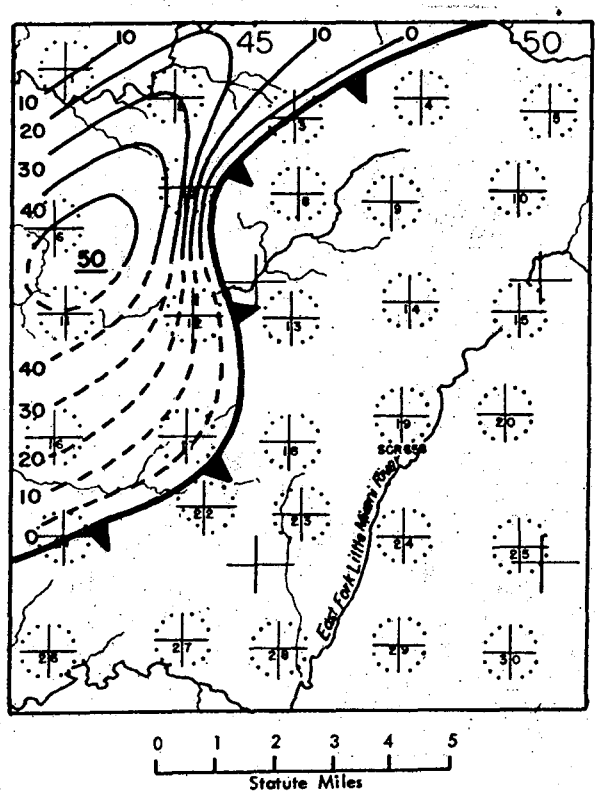

Figure 3 - Rainfall, 1355-1400 EST, March 19, 1948.

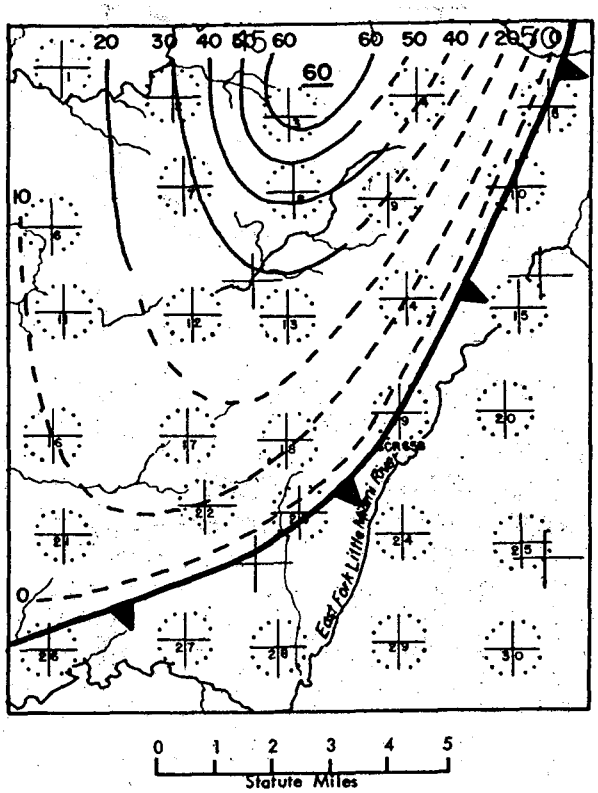

Figure 4 - Rainfall, 1400-1405 EST, March 19, 1948.

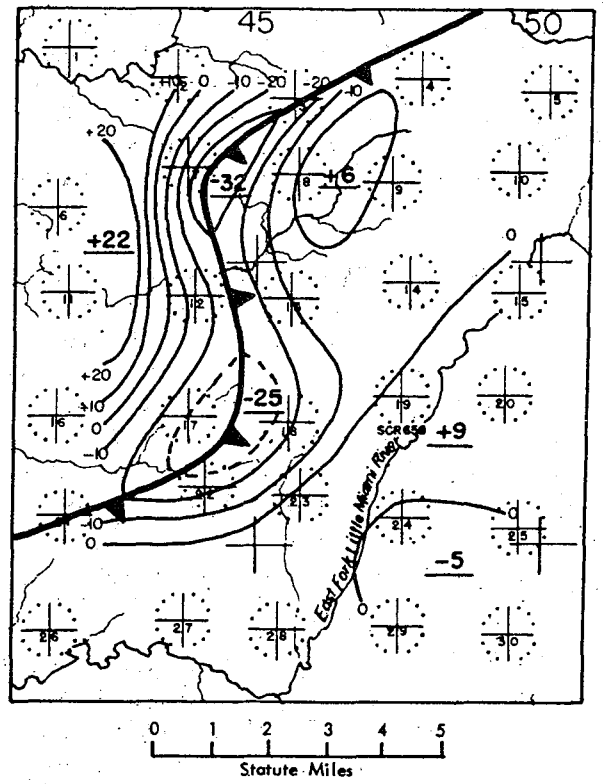

Figure 5 - $Div_2 \mathbf{V}$ in hr^{-1}, 1400 EST, March 19, 1948.

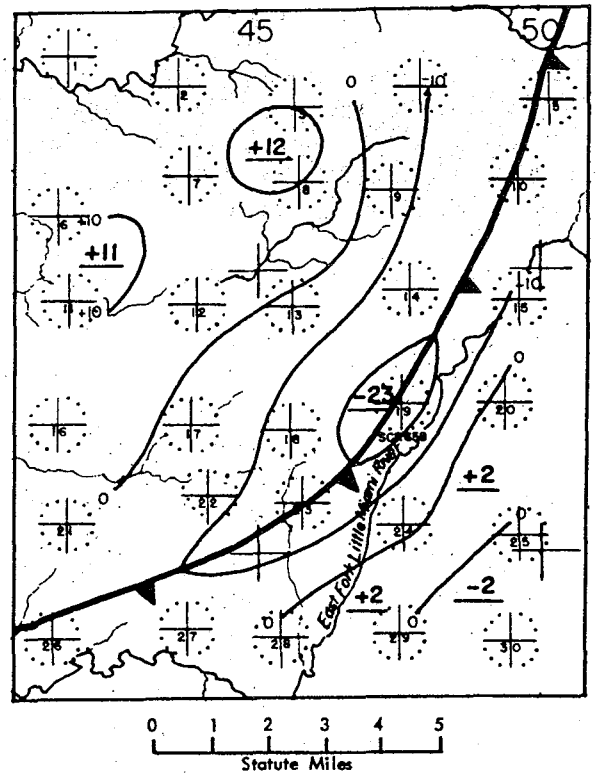

Figure 6 - $Div_2 \mathbf{V}$ in hr^{-1}, 1405 EST, March 19, 1948.

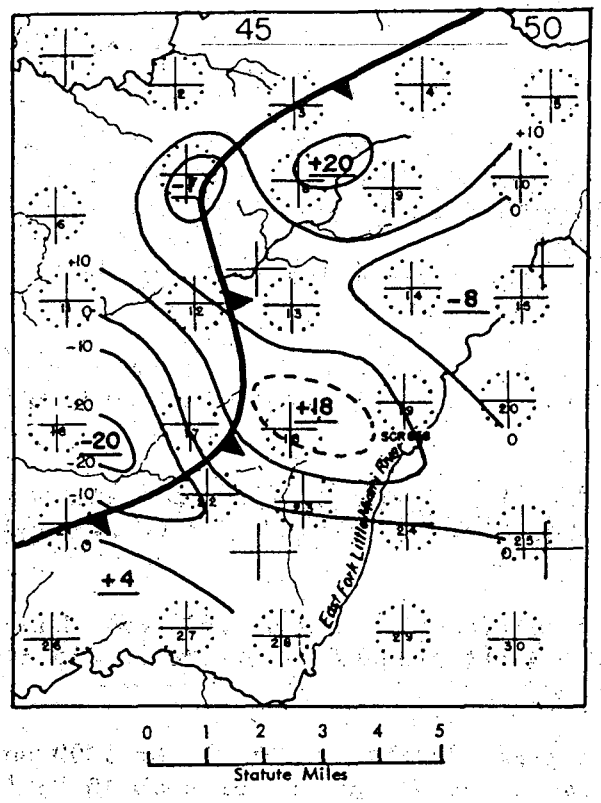

Figure 7 - $Rot_2 \mathbf{V}$ in hr^{-1}, 1400 EST, March 19, 1948.

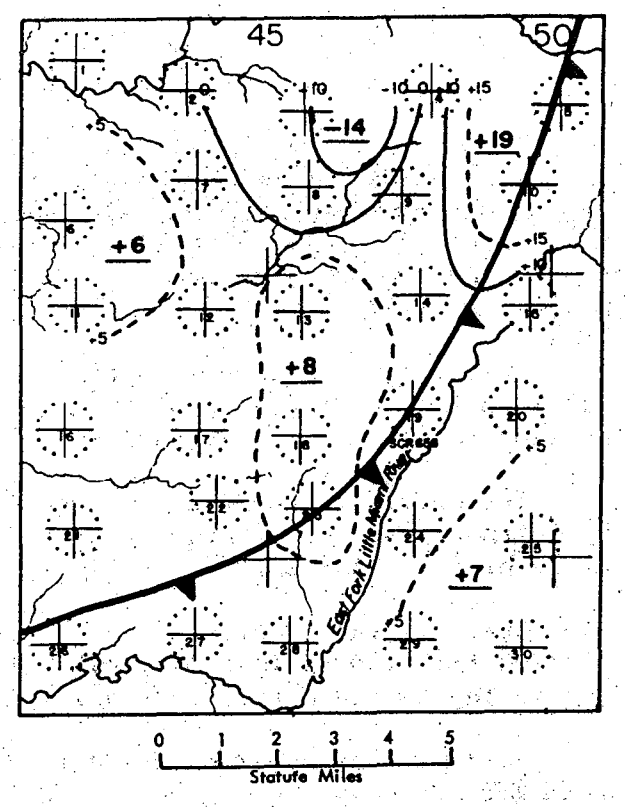

Figure 8 - $Rot_2 \mathbf{V}$ in hr^{-1}, 1405 EST, March 19, 1948.

Five-minute accumulations of rainfall in hundredths of an inch are shown in figures 3 and 4. The dashed isohyets were drawn without data. In these areas the strong winds caused the rain gage pens to vibrate excessively, and it was not possible to read off the amounts at 5-minute intervals. The intensity of the squall line is indicated by the large rainfall amounts. Centers of maximum rainfall occurred some distance to the rear of the leading edge of the squall line.

The only radar data available for this case were PPI scope photographs of the 10-cm. CPN-18 radar at Clinton County Air Force Base. This radar was located just north of the network about 4 miles north-northeast of station 3. The range of this set was only 40 miles. The photographs showed a broken to solid line of echoes oriented from north-northeast to south-southwest that passed over the station from west-northwest. Speed of movement of the line was considerably greater in its northern extremity than it was to the south. Speed 25 miles north of Clinton County Air Force Base was 30-35 m.p.h. while speed 25 miles southwest was only 5-10 m.p.h. Unfortunately ground clutter and the effects of attenuation when the line was over the station masked the features within a 10-mile radius of the station. This covered most of the area of interest, so little detail of the echo could be obtained. For this reason a plot of the echoes is not shown. However, the line of echoes showed a reasonable fit to the analyzed positions of the squall line, except that the leading edge of the line of echoes was 1 to $1\frac{1}{2}$ miles to the rear of the analyzed leading edge. This appears to be consistent with the tendency of the leading edge to run ahead of the active portion of the squall line. However, it might have resulted from the low power of the set; only the more intense portions of the squall line would have returned echoes.

Horizontal Velocity Divergence: Charts of Div_2 **V** for 1400 and 1405 EST are shown in figures 5 and 6. Isopleths are drawn for each 10 $hr.^{-1}$

The leading edge of the squall line lay in a narrow zone (2 to 4 miles wide) of intense convergence (negative divergence) with a maximum of 32 $hr.^{-1}$ in the micro-low portion at 1400 EST. A secondary maximum of 25 $hr.^{-1}$ was present about 5 miles south of the micro-low. The second maximum was conserved on the chart for 1405 EST, but the first maximum was lost, as the micro-low filled.

Positive divergence was present in the corridor in advance of and parallel to the leading edge of the squall line with values ranging up to 9 $hr.^{-1}$ at 1400 EST and 2 $hr.^{-1}$ at 1405 EST.

The micro-high behind the leading edge of the squall line was featured by intense positive divergence with maximum values of 22 $hr.^{-1}$ at 1400 EST and of 12 $hr.^{-1}$ at 1405 EST.

Over-all values of divergence were significantly less at 1405 EST than at 1400 EST, indicating the rapid but systematic changes occurring in the system in the 5-minute time interval.

Vertical Component of Relative Vorticity: Charts of Rot_2 **V** for 1400 and 1405 EST are shown in figures 7 and 8. Isopleths are drawn for each 10 $hr.^{-1}$

Fields of cyclonic (positive values) and anticyclonic (negative values) vorticity had little apparent relationship to the leading edge of the squall line, micro-low, and micro-high; and there was no simple continuity in the fields from 1400 to 1405 EST. Oddly enough the micro-low portion of the squall line at 1400 EST was featured by slight anticyclonic vorticity, although centers of maximum cyclonic vorticity were present some distance to the northeast and southeast.

Extreme dynamic instability was indicated locally and briefly with threshold values of anticyclonic vorticity exceeded by as much as a factor of 50. Threshold values are those numerically equal to the Coriolis parameter.

Isotherm Fields and Axes of Dilatation: Isotherm fields and axes of dilatation are shown in figures 9 and 10. Isotherms are drawn for every 2°F. with warm and cold centers indicated. Axes of dilatation are indicated by double-headed arrows. Axes of contraction (not indicated) are normal to the axes of dilatation.

The environmental temperature at both 1400 and 1405 EST was 72°F. At 1400 EST a cold center of 64°F. was present immediately to the northwest of the micro-low. The gradient of temperature across the leading edge of the squall line was most intense in the vicinity of the micro-low. By 1405 EST the leading edge of the squall line had advanced into the environmental temperature field in the northern portion of the network with the strong gradient of temperature lagging 2 to 4 miles behind. The cold center had intensified to 58°F. but had drifted south-southwestward. The advance of the leading edge of the squall line beyond the intense gradient of temperature may well be the reason for the filling of the micro-low and the weakening of the squall line. It is indicated that small segments of squall lines may grow and intensify as cold air is produced, and that dissipation takes place when the leading edge outruns the temperature gradient.

Dilatation axes were generally parallel to the squall line in a narrow zone on either side of its leading edge. Dilatation axes in the corridor in advance of and parallel to the leading edge were generally normal to the squall line, and the same was true in the micro-high portion behind the squall line.

Absolute Magnitude of the Resultant Deformation: Charts of Def_R **V** are shown in figures 11 and 12. Isopleths are drawn for each 10 $hr.^{-1}$.

The leading edge of the squall line lay in a narrow zone of intense deformation with a maximum value of 41 $hr.^{-1}$ in the micro-low portion at 1400 EST. This maximum was lost on the 1405 EST chart, but a maximum of 21 $hr.^{-1}$ was present farther south along the leading edge. The corridor in advance of the leading edge of the squall line was featured by minimum deformation, as was the micro-high behind the leading edge.

Values of deformation were significantly less at 1405 EST than at 1400 EST, indicating the rapid changes occurring as the micro-low filled and the squall line weakened.

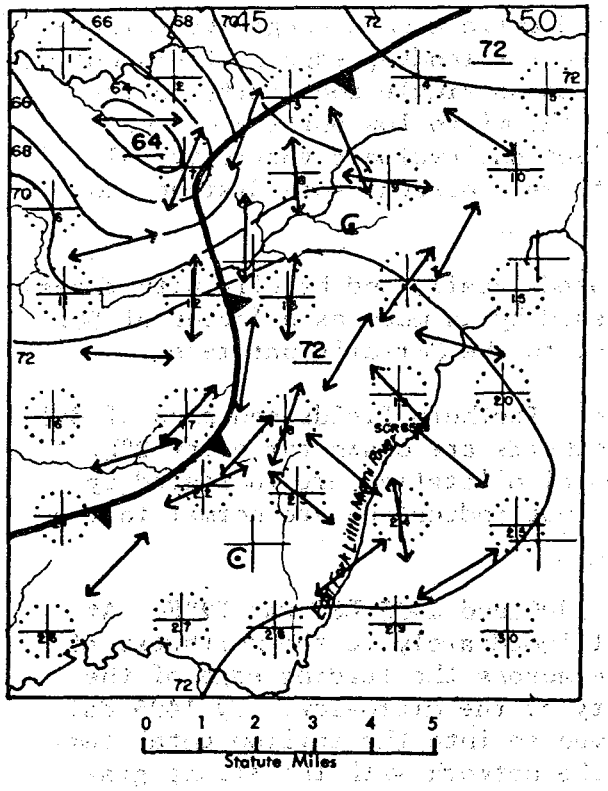

Figure 9 - Isotherms in °F and Axes of Dilatation, 1400 EST, March 19, 1948.

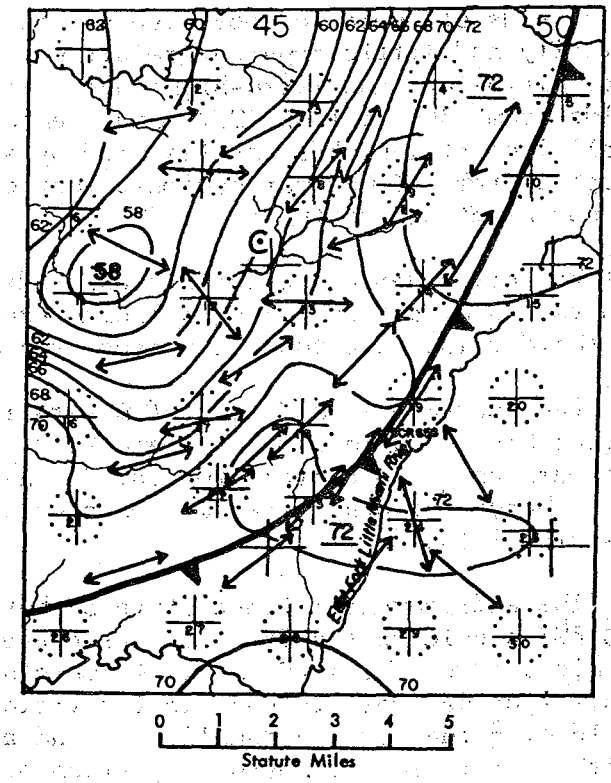

Figure 10 - Isotherms in °F and Axes of Dilatation, 1405 EST, March 19, 1948.

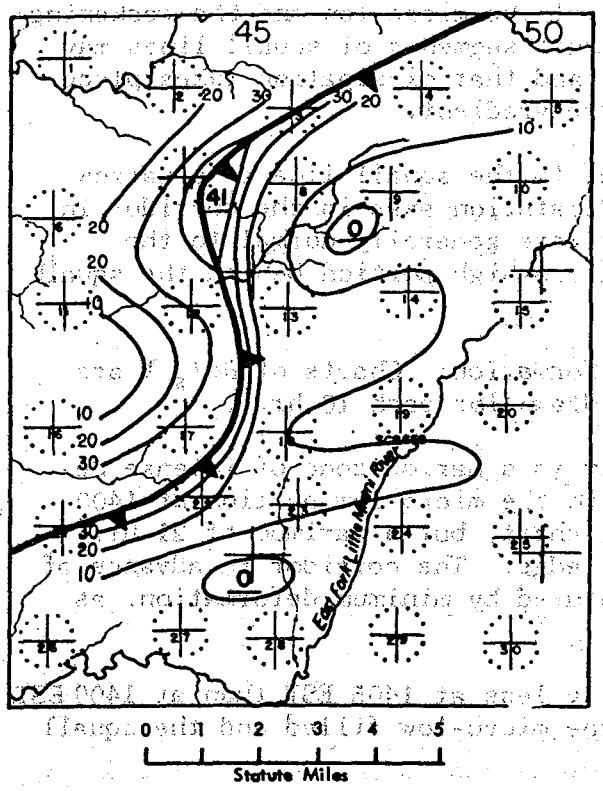

Figure 11 - Absolute Magnitude of $Def_R V$, 1400 EST, March 19, 1948.

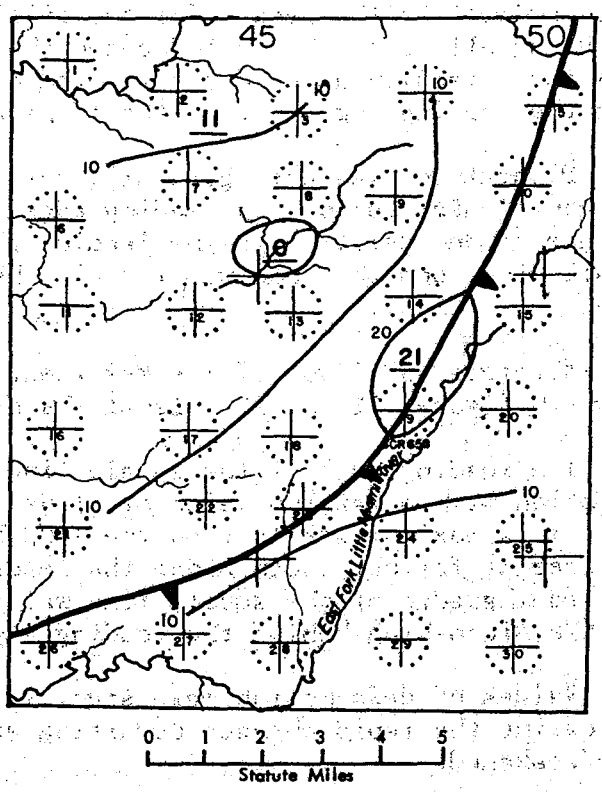

Figure 12 - Absolute Magnitude of $Def_R V$, 1405 EST March 19, 1948.

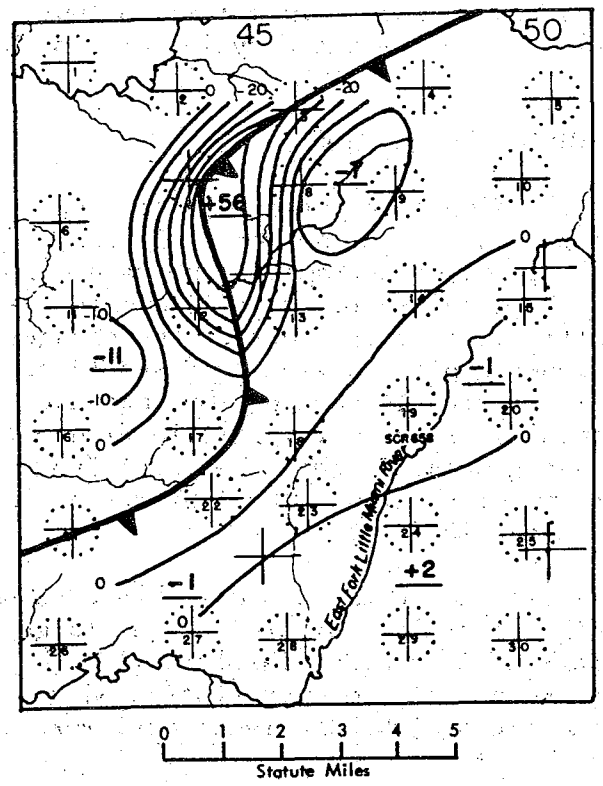

Figure 13 - Petterssen's Frontogenetical Function in °F/mi hr, 1400 EST, March 19, 1948.

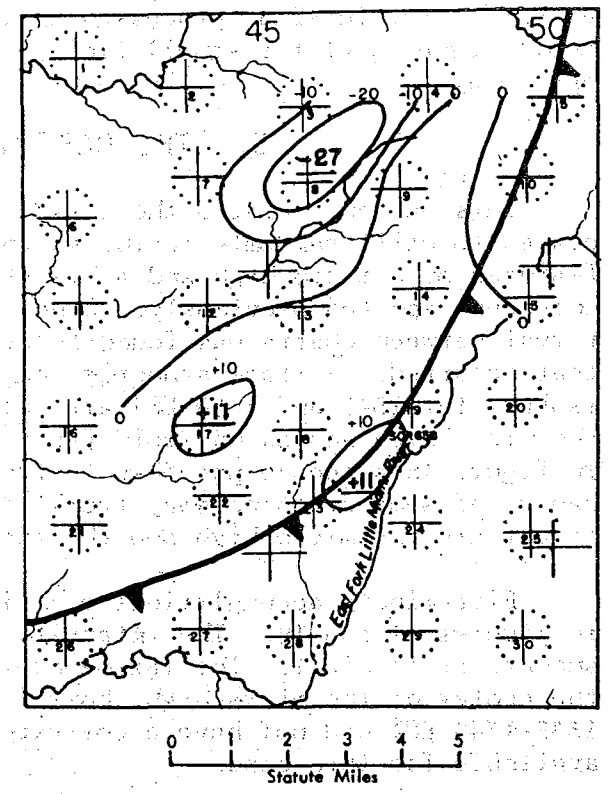

Figure 14 - Petterssen's Frontogenetical Function in °F/mi hr, 1405 EST, March 19, 1948.

Frontogenesis and Frontolysis: Charts of Petterssen's frontogenetical function are shown in figures 13 and 14. Isopleths are drawn for each 10°F. $mi.^{-1}$ $hr.^{-1}$

At 1400 EST the leading edge of the squall line lay in a narrow zone of intense frontogenesis with a maximum value of 56°F. $mi.^{-1}$ $hr.^{-1}$ in the micro-low portion. This maximum had disappeared by 1405 EST, and the leading edge of the squall line then lay in a region of almost no frontogenesis in the northern portion of the network. Maximum frontogenesis at this time was actually 1 to 2 miles to the rear of the leading edge.

Slight frontolysis (negative frontogenesis) was present in the corridor in advance of and parallel to the leading edge of the squall line at 1400 EST. Intense frontolysis, ranging up to 27°F. $mi.^{-1}$ $hr.^{-1}$ was present in portions of the micro-high behind the leading edge of the squall line.

Although convergence and deformation fields were still favorable for frontogenesis along the leading edge of the squall line at 1405 EST, the fact that the temperature gradient lagged behind these fields resulted in a great decrease in the frontogenesis. It is indicated that the growth and decay of small segments of the squall line are directly related to the intensity of frontogenesis, and that the frontogenesis is critically dependent upon the degree to which favorable convergence, deformation, and temperature gradient fields may coincide. The degree of coincidence may be determined to a large

extent by the internal processes of individual thunderstorm cells, so that small segments of the squall line progress through repeated cycles of growth and decay.

5. THE CASE OF AUGUST 29, 1948

This was an isolated thunderstorm of considerable intensity which appeared to drift randomly in the southern portion of the network. It was featured by a micro-high and at least two pseudo-cold fronts. The case has not been reported previously. Since the storm moved slowly, a 10-minute interval between charts was found to be sufficiently short to show the changes that occurred. Surface synoptic charts showing plotted winds and sea-level isobars for 1540 and 1550 EST are shown in figures 15 and 16. One may note the micro-high and pseudo-cold front partially circumscribing it in figure 15. In figure 16 a second pseudo-cold front was generated, when the first front had moved some distance away from the parent micro-high. The features of interest are the micro-high and the two pseudo-cold fronts.

Five-minute accumulations of rainfall in hundredths of an inch are shown in figures 17 and 18. The intensity of the storm is indicated by the large amounts of rainfall. The maxima near station 42 coincide fairly well with the center of the micro-high; however, a second maximum near station 54 at 1535-1540 EST did not have a corresponding micro-high. No radar data were available for this case.

Horizontal Velocity Divergence: Charts of Div_2 **V** for 1540 and 1550 EST are shown in figures 19 and 20. The pseudo-cold fronts lay in zones of moderately intense convergence. Maxima were present with a value of 13 $hr.^{-1}$ on the first front at 1540 EST and values of 11 $hr.^{-1}$ and 10 $hr.^{-1}$ on the first and second fronts respectively at 1550 EST. Overall convergence on the first front weakened somewhat during the 10-minute period, while convergence intensified on the second front as it formed.

The micro-high was featured by intense divergence, which increased from a maximum value of 23 $hr.^{-1}$ at 1540 EST to 42 $hr.^{-1}$ at 1550 EST.

Vertical Component of Relative Vorticity: Charts of Rot_2 **V** for 1540 and 1550 EST are shown in figures 21 and 22. At 1540 EST the pseudo-cold front was featured by cyclonic vorticity with a maximum of 10 $hr.^{-1}$ in its northwestern portion. Intense anticyclonic vorticity with a maximum of 16 $hr.^{-1}$ was present at the eastern edge of the micro-high. The vorticity field at 1550 EST was more poorly defined. Although moderate cyclonic vorticity was present in the northern portion of the first pseudo-cold front, it was not confined to the immediate vicinity of the front. Vorticity along the second pseudo-cold front was slightly anticyclonic. Vorticity with respect to the micro-high was featured by multiple centers of both cyclonic and anticyclonic vorticity. There appears to have been little continuity in the vorticity change from 1540 to 1550 EST.

Extreme dynamic instability was indicated locally and briefly with threshold values of anticyclonic vorticity exceeded by as much as a factor of 40.

Isotherm Fields and Axes of Dilatation: Isotherm fields and axes of dilatation are shown in figures 23 and 24. The environmental temperature at both 1540 and 1550 EST was 90°F. At 1540 EST a cold center of 70°F. was present on the southeastern boundary of the network. Gradients of temperature were most intense immediately south of the pseudo-cold front. By 1550 EST a new cold center of 64°F. had formed in the western portion of the network. The gradient of temperature between this center and the warm center to the northwest was 26°F. over a distance of 4 miles! Gradients of temperature remained strong to the south of the first pseudo-cold front and were strong on either side of the second pseudo-cold front.

Dilatation axes were generally parallel to the pseudo-cold fronts in narrow zones on either side. Dilatation axes in the micro-high and some distance from the pseudo-cold fronts tended to be normal to the fronts. Dilatation axes tended to parallel the isotherms in the vicinity of the pseudo-cold fronts. They were more normal to the isotherms elsewhere.

Absolute Magnitude of the Resultant Deformation: Charts of Def_R **V** are shown in figures 25 and 26. At 1540 EST the pseudo-cold front lay in a narrow zone of intense deformation with a maximum value of 31 $hr.^{-1}$ in the northwestern portion. The deformation was at a minimum over the southeastern portion of the network. At 1550 EST deformation had decreased along the first pseudo-cold front but had increased to a maximum of 26 $hr.^{-1}$ along the second pseudo-cold front, as it formed. Another maximum of 30 $hr.^{-1}$ was present in the micro-high. Deformation was at a minimum at the south-central portion of the network.

Changes in the deformation reflect the decay of the first pseudo-cold front and the generation of the second front.

Frontogenesis and Frontolysis: Charts of Petterssen's frontogenetical function are shown in figures 27 and 28. At 1540 EST the pseudo-cold front lay in a zone of intense frontogenesis with a maximum value of 52°F. $mi.^{-1}$ $hr.^{-1}$ in the northwestern portion. However, this center of frontogenesis extended somewhat southeastward from the front, indicating the formation of a new front farther south. At 1550 EST very intense frontogenesis with a maximum value of 96°F. $mi.^{-1}$ $hr.^{-1}$ was present along the second pseudo-cold front. Meanwhile frontogenesis along the first pseudo-cold front had decreased to slightly more than 20°F. $mi.^{-1}$ $hr.^{-1}$.

The micro-high at both 1540 and 1550 EST was featured by intense frontolysis with maximum values of 52°F. $mi.^{-1}$ $hr.^{-1}$ at 1540 EST and 66°F. $mi.^{-1}$ $hr.^{-1}$ at 1550 EST.

The intense fields of frontogenesis and frontolysis resulted from the coincidence of favorable fields of divergence, deformation, and temperature gradients. The generation of a second pseudo-cold front, very markedly supported by an intense frontogenetical field, indicates that the isolated thunderstorm may generate successive pseudo-cold fronts that tend to circumscribe its micro-high. Early pseudo-cold fronts tend to weaken when they move too far from the parent storm, and they are repeatedly replaced by new and more intense pseudo-cold fronts closer in. The generation of new pseudo-cold fronts,

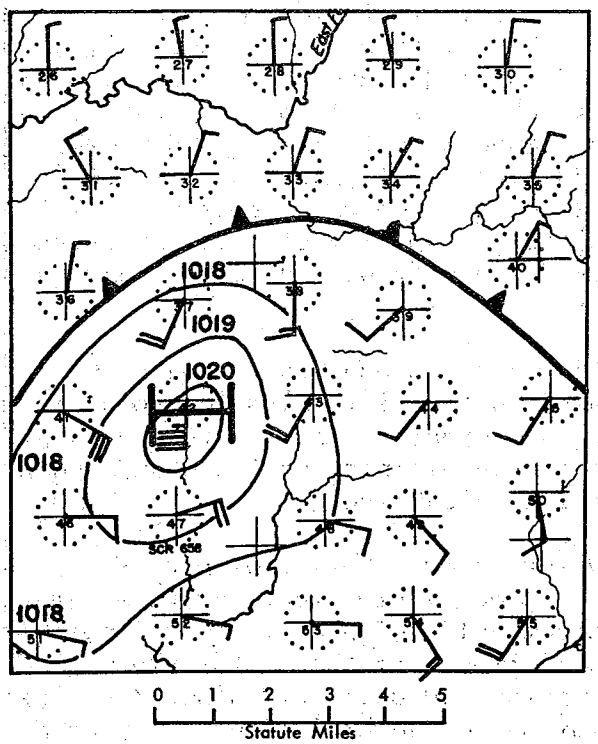

Figure 15 - Surface wind and pressure, 1540 EST, August 29, 1948.

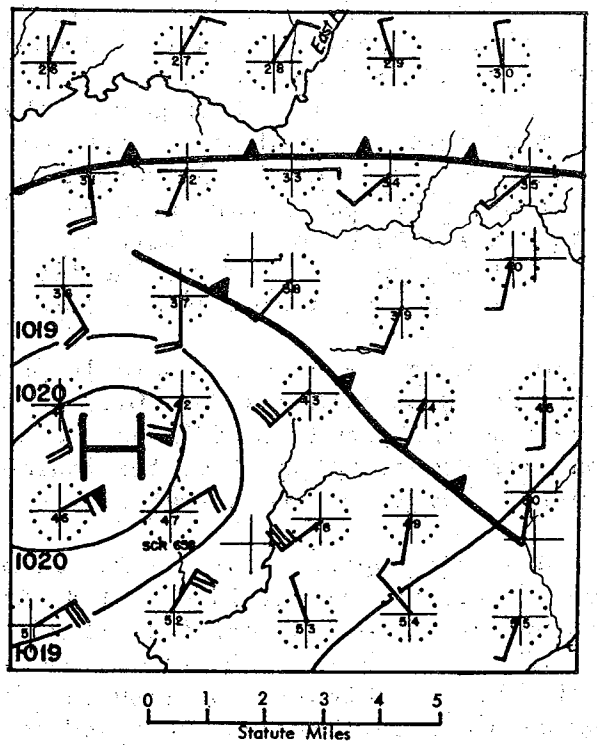

Figure 16 - Surface wind and pressure, 1550 EST, August 29, 1948.

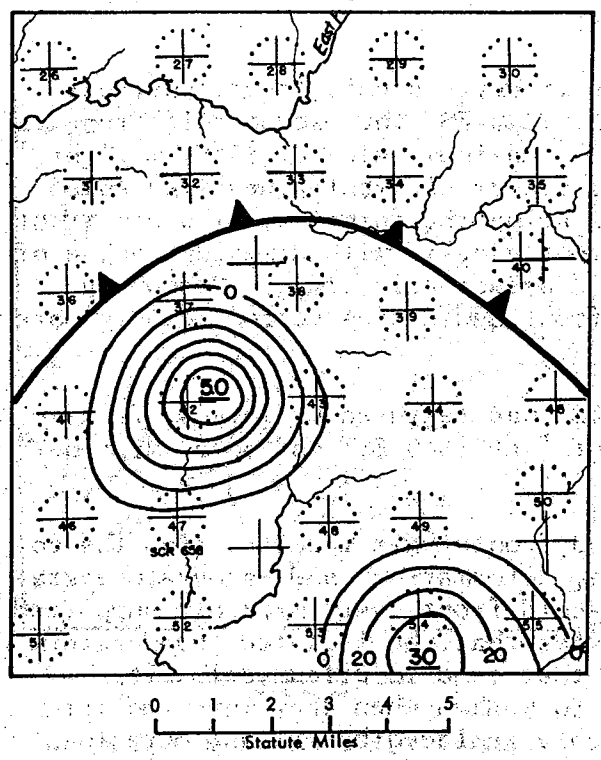

Figure 17 - Rainfall, 1535-1540 EST, August 29, 1948.

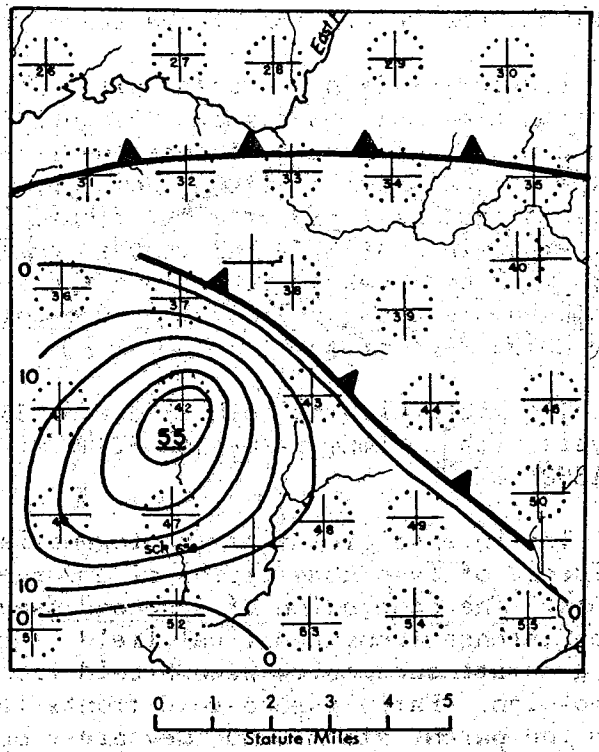

Figure 18 - Rainfall, 1545-1550 EST, August 29, 1948.

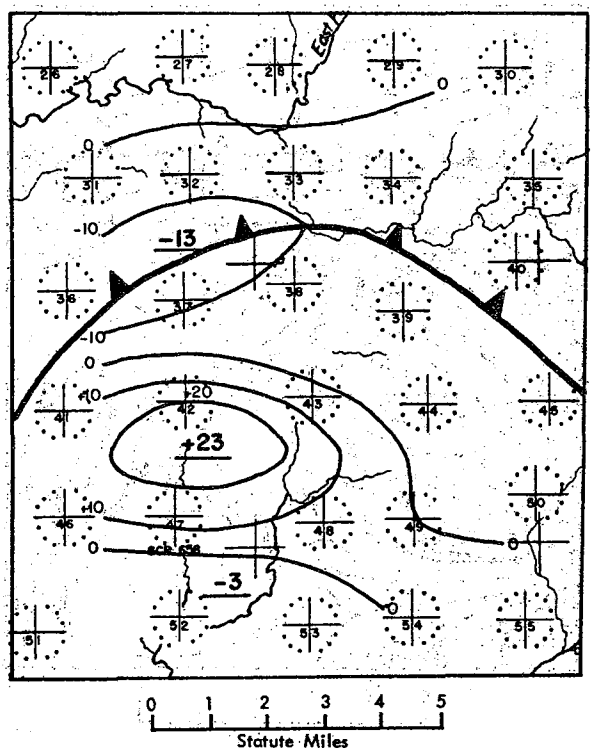

Figure 19 - $Div_2 \mathbb{V}$ in hr^{-1}, 1540 EST, August 29, 1948.

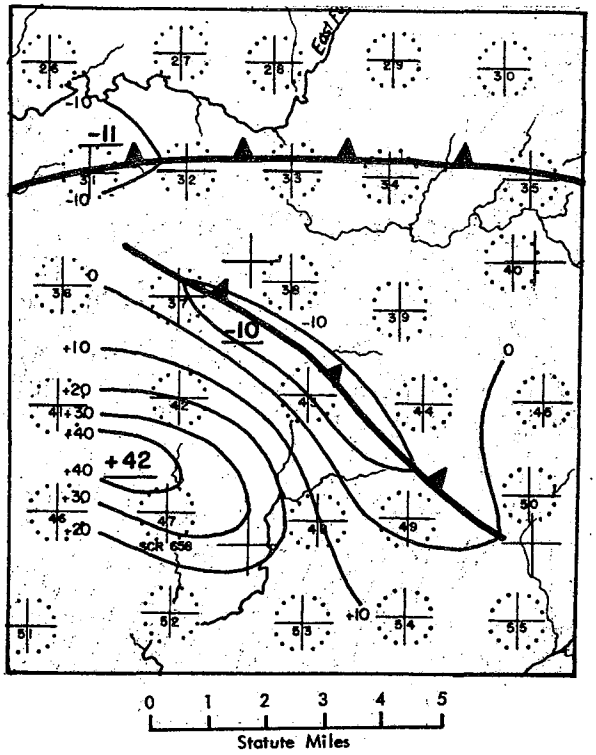

Figure 20 - $Div_2 \mathbb{V}$ in hr^{-1}, 1550 EST, August 29, 1948.

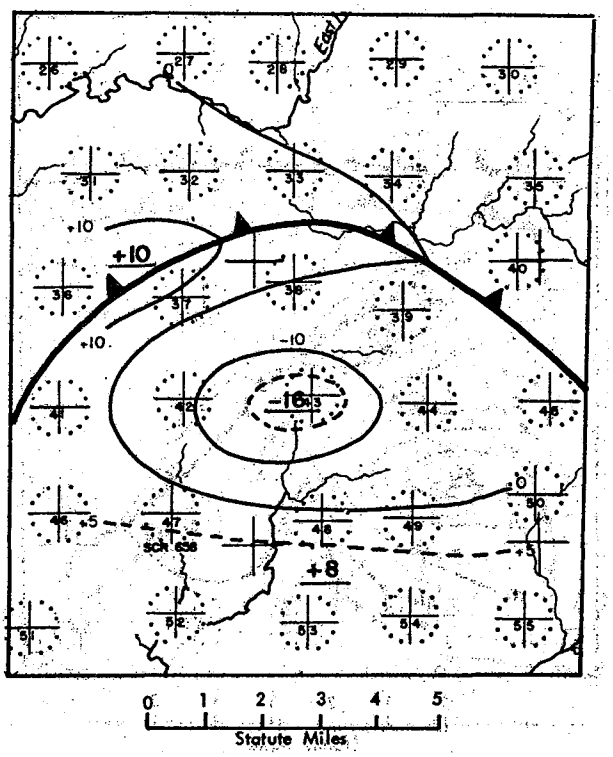

Figure 21 - $Rot_2 \mathbf{V}$ in hr^{-1}, 1540 EST, August 29, 1948.

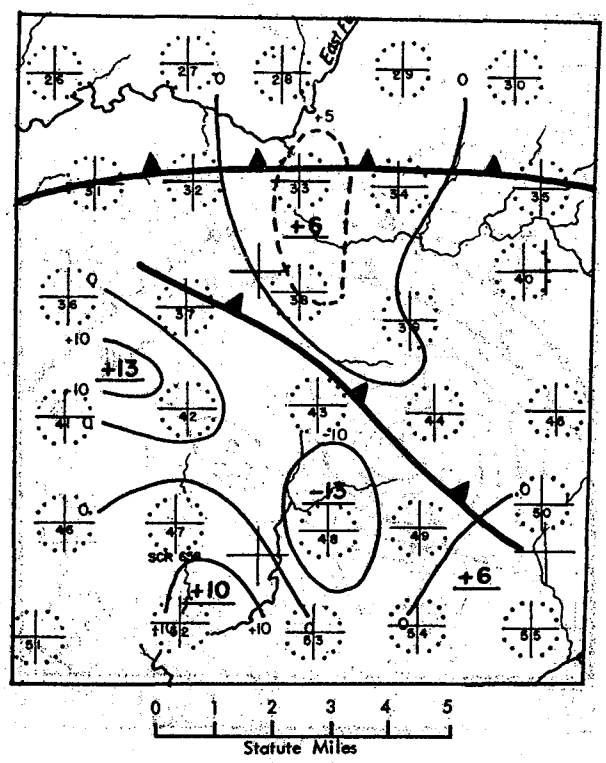

Figure 22 - $Rot_2 \mathbf{V}$ in hr^{-1}, 1550 EST, August 29, 1948.

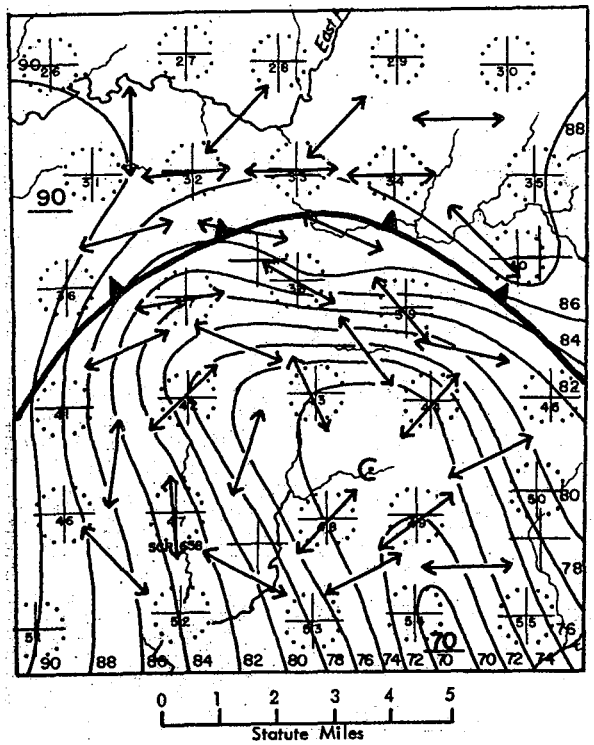

Figure 23 - Isotherms in °F and Axes of Dilatation, 1540 EST, August 29, 1948.

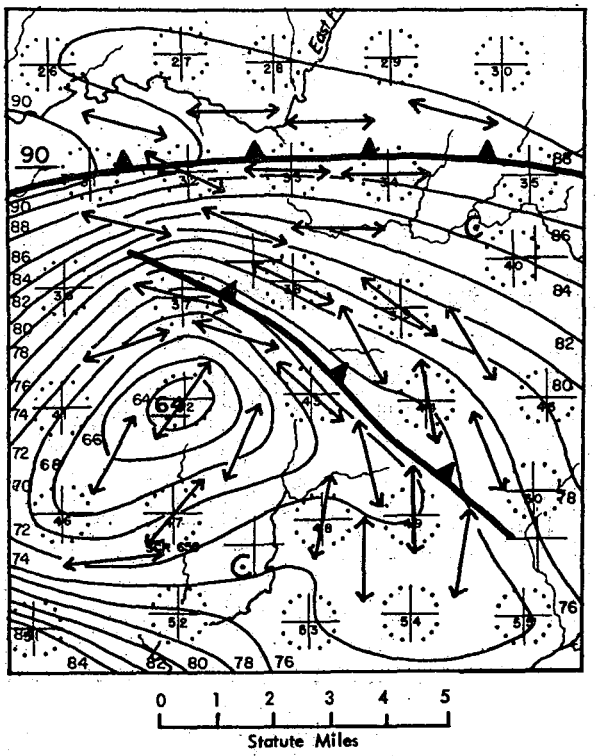

Figure 24 - Isotherms in °F and Axes of Dilatation, 1550 EST, August 29, 1948.

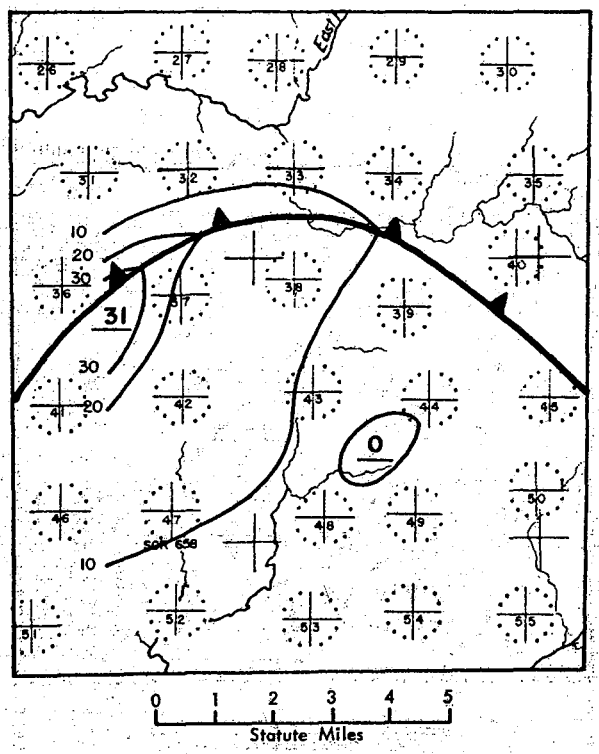

Figure 25 - Absolute Magnitude of $Def_R W$, 1540 EST, August 29, 1948.

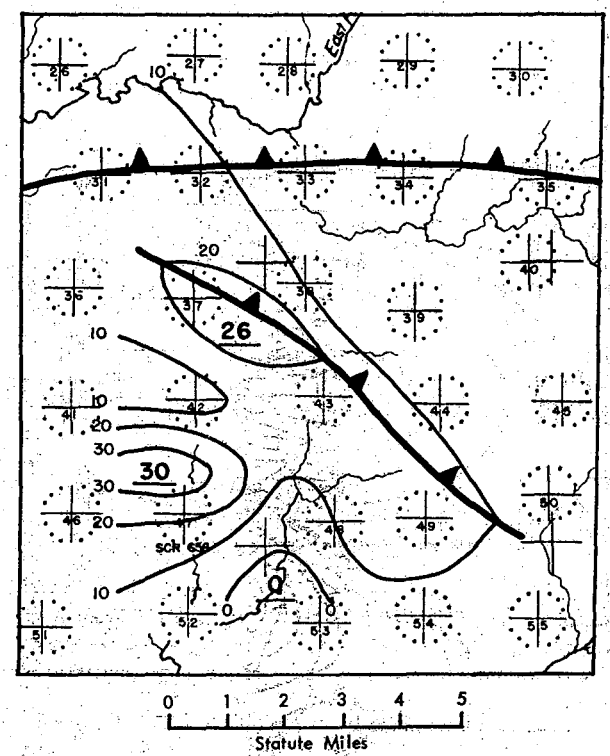

Figure 26 - Absolute Magnitude of $Def_R W$, 1550 EST, August 29, 1948.

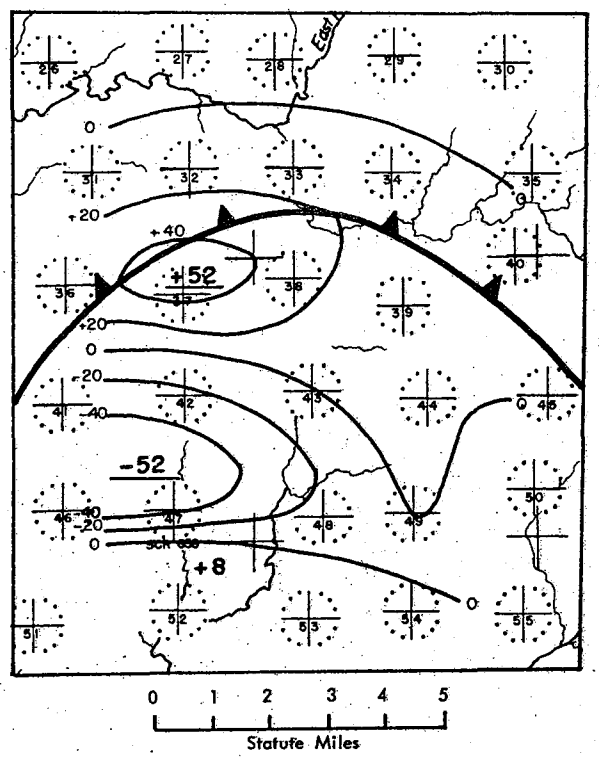

Figure 27 - Petterssen's Frontogenetical Function in °F/mi hr, 1540 EST, August 29, 1948.

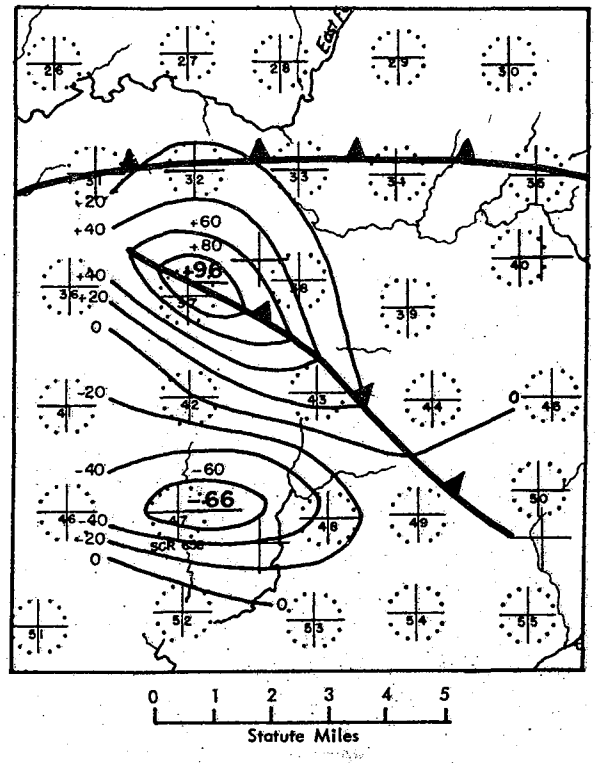

Figure 28 - Petterssen's Frontogenetical Function in °F/mi hr, 1550 EST, August 29, 1948.

as a coincidence of favorable kinematic and thermal fields, is probably linked to the internal processes of individual cells composing the thunderstorm, so that the individual pseudo-cold fronts show to a certain extent the growth and decay of individual thunderstorm cells.

6. THE CASE OF APRIL 7, 1948

This was a depression wave line, which followed but was offset from an earlier squall line. Various features of the case have been reported previously [6]. Surface synoptic charts with plotted winds and sea level isobars at 1315 and 1320 EST are shown in figures 29 and 30. The features of interest are the depression wave line (line of minimum sea level pressure, indicated as a heavy dashed line) and a micro-low (area of minimum sea level pressure).

There was no measurable rainfall over the network from 1310 to 1320 EST. Rainfall which had occurred a short time earlier had diminished to none or trace amounts, and the trace amounts occurred only in advance of the depression wave line. No radar data were available for this case.

Horizontal Velocity Divergence: Charts of Div_2 V for 1315 and 1320 EST are shown in figures 31 and 32. Isopleths are drawn for each 5 $hr.^{-1}$

Moderate values of convergence were generally present along the depression wave line. Greatest values were near, but not quite coincident with,

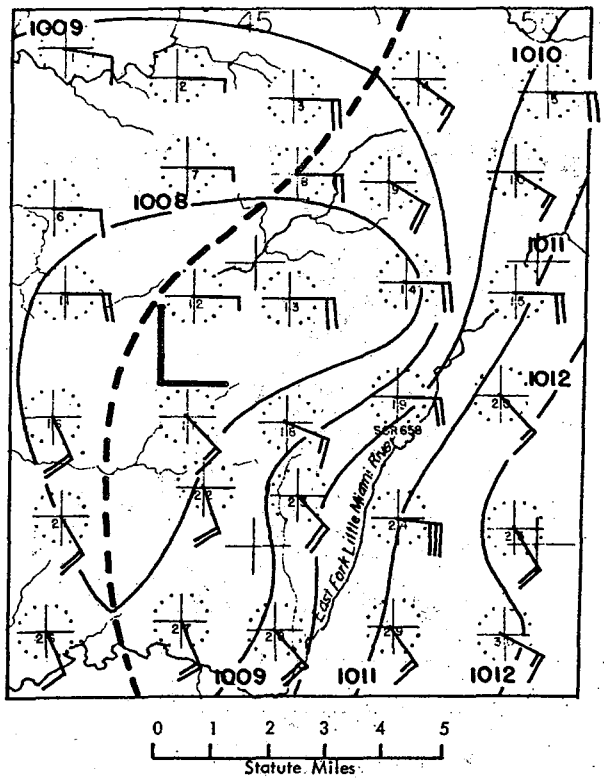

Figure 29 - Surface wind and pressure, 1315 EST, April 7, 1948.

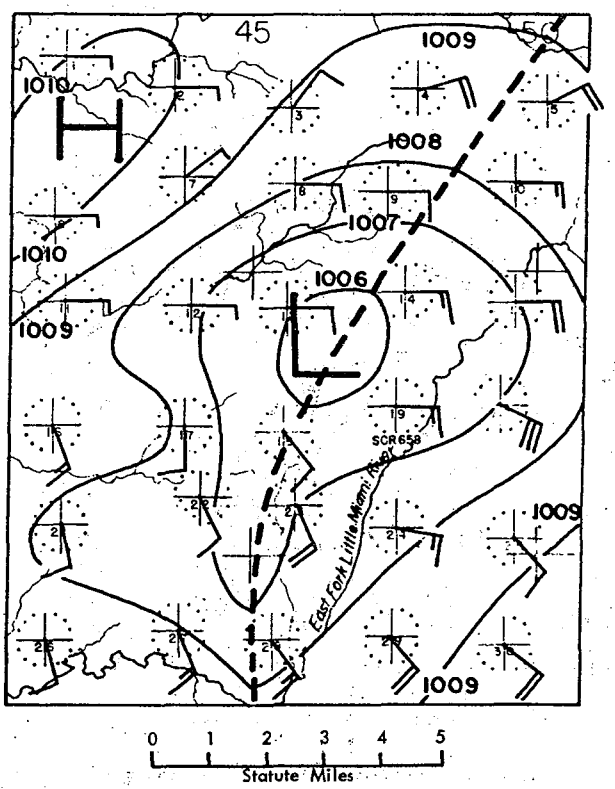

Figure 30 - Surface wind and pressure, 1320 EST, April 7, 1948.

the micro-low portion. A convergence maximum of 14 hr.$^{-1}$ at 1315 EST was located about 3 miles southeast of the micro-low. At 1320 EST a maximum of 10 hr.$^{-1}$ was located about 2 miles south of the micro-low.

Values of divergence were somewhat less than values of convergence. At 1315 EST the depression wave line was featured by a region of positive divergence some distance in advance of the line and a short distance behind the line. However, at 1320 EST the divergence was present only in the northwestern and southwestern portions of the network.

Although the fields of divergence bear some relationship to the depression wave line and the micro-low, these relationships are not so systematic or so continuous, as they were in the previous cases.

The Vertical Component of Relative Vorticity: Charts of Rot_2 **V** for 1315 and 1320 EST are shown in figures 33 and 34. Isopleths are drawn for each 5 hr.$^{-1}$.

There appears to have been no simple relationship between the vorticity field and the depression wave line. However, there was some continuity to the vorticity field. Individual maxima and minima at 1315 EST generally appeared in the same locations at 1320 EST, suggesting that the vorticity field was quasi-stationary with respect to the depression wave line moving through it.

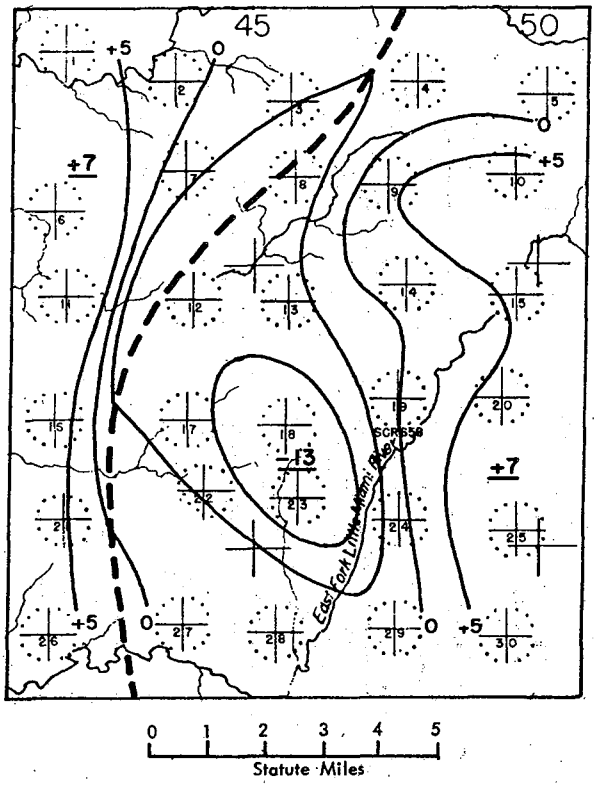

Figure 31 - $Div_2 W$ in hr^{-1}, 1315 EST, April 7, 1948.

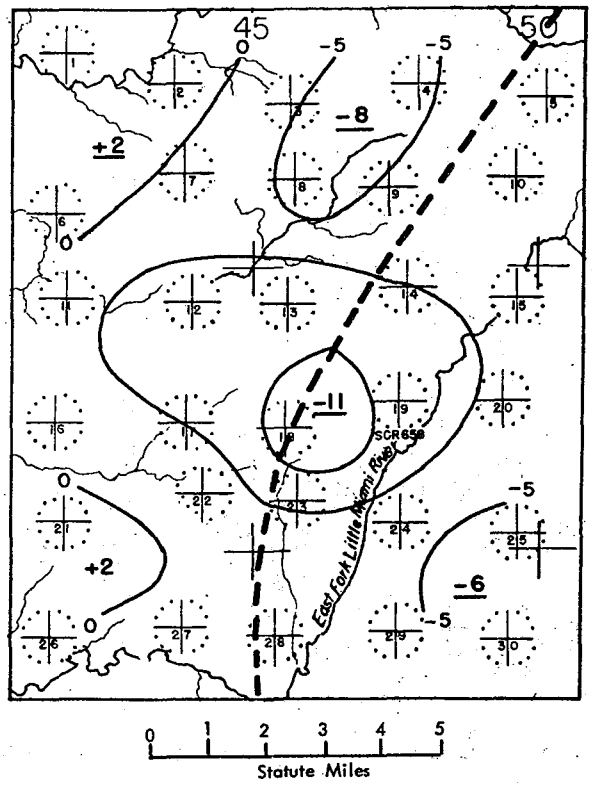

Figure 32 - $Div_2 W$ in hr^{-1}, 1320 EST, April 7, 1948.

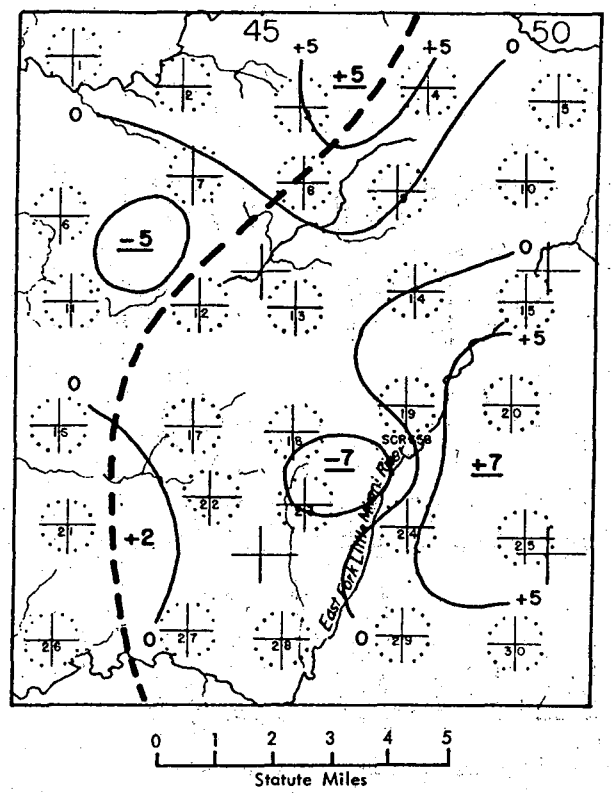

Figure 33 - $Rot_2 W$ in hr^{-1}, 1315 EST, April 7, 1948.

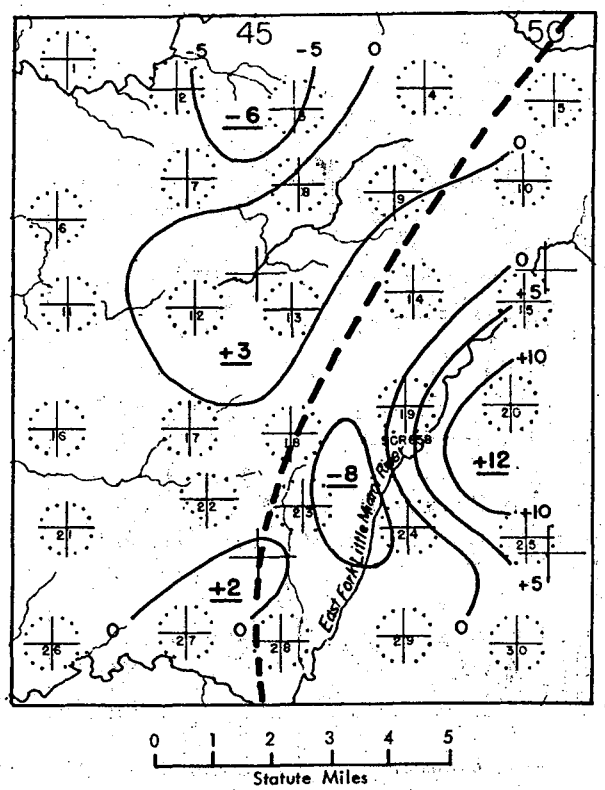

Figure 34 - $Rot_2 W$ in hr^{-1}, 1320 EST, April 7, 1948.

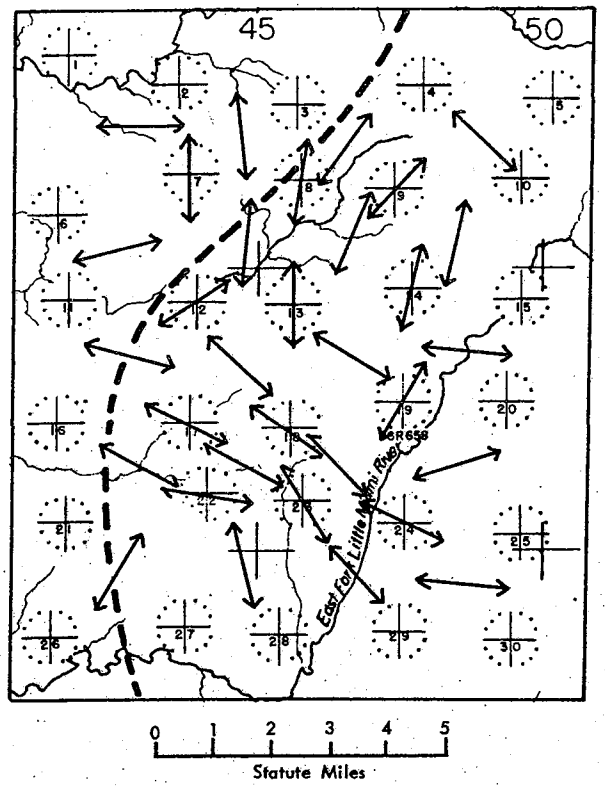

Figure 35 - Axes of Dilatation, 1315 EST, April 7, 1948.

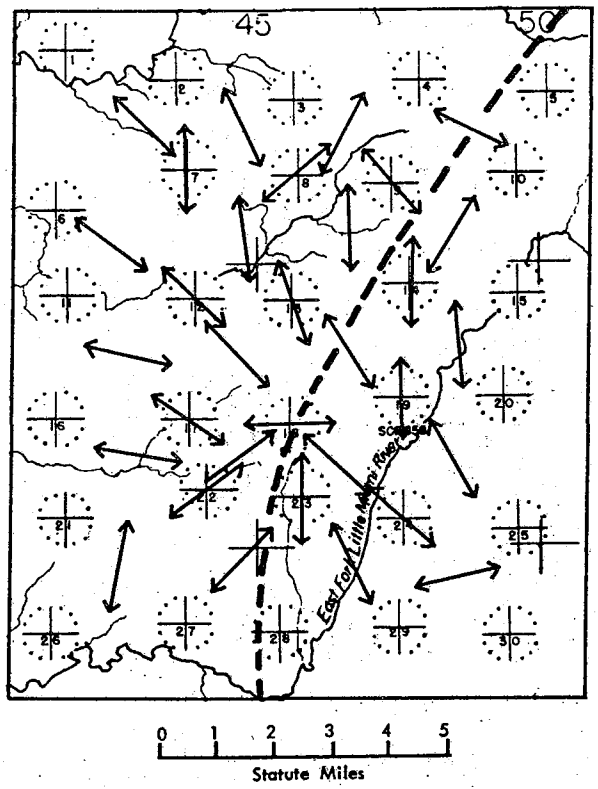

Figure 36 - Axes of Dilatation, 1320 EST, April 7, 1948.

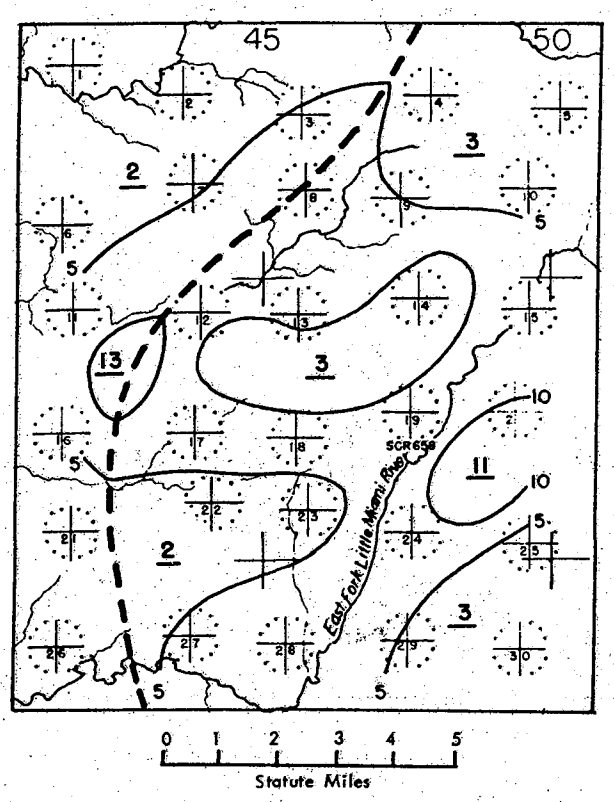

Figure 37 - Absolute Magnitude of $Def_R W$, 1315 EST, April 7, 1948.

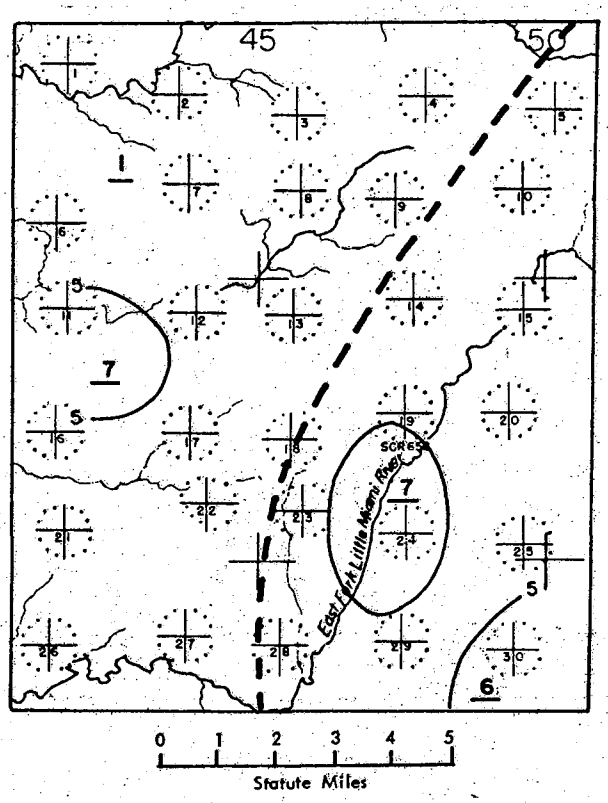

Figure 38 - Absolute Magnitude of $Def_R W$, 1320 EST, April 7, 1948.

Extreme dynamic instability was indicated locally and briefly with threshold values of anticyclonic vorticity exceeded by as much as a factor of 20.

Isotherm Fields and Axes of Dilatation: Axes of dilatation are shown in figures 35 and 36. The temperature over the network at both 1315 and 1320 EST ranged only from 58° to 59°F. The gradients were too slight to permit the drawing of isotherms. The absence of a strong gradient of temperature with respect to the depression wave line is not necessarily typical. Cases (especially those occurring at night) have been investigated in which marked temperature rises have occurred with the depression wave line.

Although there were some areas in which the dilatation axes lay either parallel or normal to the depression wave line, there appears to have been no systematic relationship to the line as a whole. It is concluded that the axes of deformation are less systematic with respect to the depression wave line than with respect to the other systems studied.

Absolute Magnitude of the Resultant Deformation: Charts of Def_R V are shown in figures 37 and 38. Isopleths are drawn for each 5 $hr.^{-1}$

Although moderate values of deformation were present, they were rather poorly related to the depression wave line and the micro-low. Moreover, the continuity of the deformation field from 1315 to 1320 EST is also poor. It is concluded that the absolute magnitude of the resultant deformation is less systematic with respect to the depression wave line than with respect to the other systems studied.

Frontogenesis and Frontolysis: Charts of Petterssen's frontogenetical function are not shown. The frontogenetical function was negligibly small, since the temperature gradients were negligibly small. However, as pointed out earlier, some depression waves are featured by temperature rises. If such had been the case here, then frontogenesis, specifically warm frontogenesis, would have been present in portions of the network.

7. SUMMARY

A. *General Features*

1. Kinematic properties of the squall line, isolated thunderstorm, and depression wave line were 2 to 3 orders of magnitude greater than those normally measured on the gross synoptic scale. Although the large values resulted from the small measuring interval used, they are believed to approximate the true values that were present in the systems studied.

2. All of the kinematic properties, excepting vorticity, were systematically related to the small-scale features of the squall line and isolated thunderstorm. Great but systematic changes in the properties occurred in the 5- to 10-min. intervals between charts.

3. The relationships of the kinematic properties to the small-scale features of the depression wave line were less systematic than those of the squall line and isolated thunderstorm.

4. Vorticity fields were poorly related to the small-scale systems, and the continuity of vorticity features from one time to the next was poor. It is indicated that small-scale systems may have no typical vorticity fields.

5. Extreme dynamic instability was present with threshold values of anticyclonic vorticity locally and briefly exceeded by as much as a factor of 50.

B. *Specific Features of the Squall Line*

1. The leading edge of the squall line lay in a narrow zone of intense convergence, deformation, and frontogenesis. Axes of dilatation were generally parallel to the leading edge of the squall line.

2. The micro-low portion of the squall line was an area of maximum convergence, frontogenesis, and deformation. Vorticity was slightly anticyclonic in the micro-low.

3. The micro-low filled and the squall line weakened, when frontogenesis decreased. The decrease in frontogenesis occurred when the convergence and deformation fields of the squall line advanced beyond the zone of the intense temperature gradient.

4. A narrow corridor, characterized by slight to moderate divergence and frontolysis, and with dilatation axes generally normal to the squall line, was present in advance of and parallel to the leading edge of the squall line.

5. The micro-high behind the leading edge of the squall line was an area of intense divergence and frontolysis with dilatation axes generally normal to the squall line.

6. Very heavy rainfall occurred behind the leading edge of the squall line with the maximum rate some distance to the rear of the leading edge.

C. *Specific Features of the Isolated Thunderstorm*

1. The isolated thunderstorm was featured by a micro-high and pseudo-cold fronts partially circumscribing the micro-high.

2. The pseudo-cold fronts lay in zones of intense convergence, frontogenesis, and deformation. Axes of deformation were generally parallel to the pseudo-cold fronts.

3. Convergence, deformation, and frontogenesis decreased along the first pseudo-cold front as it moved away from the micro-high. It was replaced by a second pseudo-cold front at closer proximity to the micro-high. Convergence, deformation, and frontogenesis increased rapidly along the second pseudo-cold front as it formed.

4. The micro-high of the isolated thunderstorm was an area of very heavy rainfall, and intense divergence and frontolysis with dilatation axes generally normal to the pseudo-cold fronts.

D. *Specific Features of the Depression Wave Line.*

1. Only traces of rainfall occurred in the vicinity of the depression wave line, and these occurred only in advance of the line.

2. Although the depression wave line and its micro-low lay generally in an area of convergence, the convergence and divergence fields were rather poorly defined.

3. Vorticity and deformation fields were quite poorly defined with respect to the depression wave line and its micro-low.

4. The gradient of temperature was negligibly small with respect to the depression wave line. Because of this the frontogenetical function was also negligibly small.

8. ACKNOWLEDGMENTS

The author desires to acknowledge the guidance and encouragement of Mr. C. F. Van Thullenar, Director, and Dr. C. W. Newton, Chief Scientist, in the preparation of this paper.

REFERENCES

1. Saucier, W. J.,"Kinematic Analysis," *Principles of Meteorological Analysis*, The University of Chicago Press, Chicago, Ill., 1955, pp. 355-363.

2. Petterssen, S., "Fronts and Frontogenesis," *Weather Analysis and Forecasting, Vol. 1: Motion and Motion Systems*, McGraw-Hill Book Co., New York, N. Y., 1956, pp. 200-202.

3. Williams, D. T., "A Surface Micro-Study of Squall-Line Thunderstorms," *Monthly Weather Review*, vol. 76, No. 11, Nov. 1948, pp. 239-246.

4. Williams, D. T., "A Method for Computing Small-Scale Divergence Along a Wind Shift Line," *Bulletin of the American Meteorological Society*, vol. 41, No. 7, July 1960, pp. 383-385.

5. Williams, D. T., "A Theoretical Estimate of Draft Velocities in a Severe Thunderstorm," *Monthly Weather Review*, vol. 87, No. 2, Feb. 1959, pp. 65-68.

6. Williams, D. T., "A Surface Study of a Depression-Type Wave," *Monthly Weather Review*, vol. 82, No. 10, Oct. 1954, pp. 289-295.

USCOMM-WB-DC